ADVANCED HEALTHCARE MATERIALS
www.advhealthmat.de

Brain Microenvironment Responsive and Pro-Angiogenic Extracellular Vesicle-Hydrogel for Promoting Neurobehavioral Recovery in Type 2 Diabetic Mice After Stroke

Yixu Jiang, Ruiqi Wang, Cheng Wang, Yiyan Guo, Tongtong Xu, Zhijun Zhang, Guo-Yuan Yang, He Xu, and Yaohui Tang**

Stroke patients with diabetes have worse neurological outcomes than non-diabetic stroke patients, and treatments beneficial for non-diabetic stroke patients are not necessarily effective for diabetic stroke patients. While stem cell-derived extracellular vesicles (EVs) show potential for treating stroke, the results remain unsatisfactory due to the lack of approaches for retaining and controlling EVs released into the brain. Herein, a glucose/reactive oxygen species dual-responsive hydrogel showing excellent injectability, biocompatibility, and self-healing capability is introduced as an EVs-loading vehicle and an intelligent EVs sustained releasing system in the brain. These EVs-hydrogels are developed via crosslinking of phenylboronic acid-modified hyaluronic acid and Poly vinyl alcohol, and fusion with neural stem cell-derived EVs. The results show EVs are stably incorporated into the hydrogels and can be controllably released in response to the brain microenvironment after stroke in type 2 diabetic mice. The EVs-hydrogels exert an excellent angiogenic effect, increasing the migration and tube formation of human umbilical vein endothelial cells. In addition, injection of EVs-hydrogels into the ischemic mouse brain enhances EVs retention and facilitates sustained release, promotes angiogenesis, and improves neurobehavioral recovery. These results suggest such a microenvironment responsive and sustained release EVs-hydrogel system offers a safe, and efficient therapy for diabetic stroke.

1. Introduction

Stroke is the second leading cause of death and the first cause of disability in the world. Diabetes mellitus (DM) is one of the major risk factors for stroke.[1] Approximately 30% of stroke patients are reported to have DM, and the risk of ischemic stroke is more than doubled in patients with diabetes compared to individuals without diabetes.[2] In addition, diabetes alters metabolism, affects vasculature, and increases inflammation, resulting in complicated stroke pathology and aggravated vascular and white matter damage after stroke.[3] Thus, diabetic stroke patients have worse neurological outcomes than non-diabetic stroke patients. However, effective therapies for stroke patients with diabetes are limited. The classic pharmacological option to treat diabetic stroke is insulin with tissue plasminogen activator (t-PA).[4] Although this kind of treatment lowers the incidence of hemorrhagic transformation (HT), numerous studies have shown that maintaining glycemic balance is essential for achieving the therapeutic effect of diabetic stroke.[5] Excessive lowering of hyperglycemia by using insulin was found to increase infarct size and cause hypoglycemic events.[6] To date, all Phase III clinical trials utilizing neuroprotective agents have failed except for t-PA thrombolysis. Meanwhile, it has been demonstrated that diabetic stroke animals exhibit resistance to thrombolytic therapy and are prone to a cerebral hemorrhage.[7] Since reactive oxygen species (ROS) and high blood glucose greatly affect the recovery of stroke, it is important to develop novel therapies for treating ischemic stroke especially in the diabetic population.

Accumulating evidence suggests that stem cell-based neurorestorative therapies have great potential in treating stroke patients with or without diabetes. For example, administration of neural stem cells (NSCs) into ischemic mice improves neuroplasticity and neurological outcomes by differentiating into neurons to replace dead neurons or stimulating restorative processes such as neurogenesis and angiogenesis through their paracrine effects.[8] However, translation of NSCs-based therapies into

Y. Jiang, C. Wang, Y. Guo, T. Xu, Z. Zhang, G.-Y. Yang, Y. Tang
Shanghai Jiao Tong University Affiliated Sixth People's Hospital
School of Biomedical Engineering
Shanghai Jiao Tong University
1954 Hua Shan Road, Shanghai 200030, China
E-mail: yaohuitang@sjtu.edu.cn
R. Wang, H. Xu
College of Chemistry and Materials Sciences
Shanghai Normal University
No.100 Guilin Road, Shanghai 200234, China
E-mail: xuhe@shnu.edu.cn

The ORCID identification number(s) for the author(s) of this article can be found under https://doi.org/10.1002/adhm.202201150

DOI: 10.1002/adhm.202201150

the clinic remains challenging due to the high mortality of administrated NSCs, off-targeting issues, and potential side effects including immune-mediated rejection risk and potential tumorigenicity risk.[9] Recent studies have shown that the NSC-mediated paracrine effect, rather than differentiation, is the main mechanism exerting their role in promoting neurological recovery after stroke.[10] Extracellular vesicles (EVs) are small vesicles that contain proteins, lipids, and genetic materials, play a major role in cell-cell communication. A study comparing the therapeutic effects of stem cells with stem cell-derived EVs showed that both treatments improved angiogenesis in the ischemic brain with no significant difference between stem cell treatment and stem cell-derived EVs treatment.[11] These findings suggest that EVs have therapeutic potential to replace stem cells. Thus, EVs-based therapy holds great promise as an ideal approach to promote brain repair after stroke. However, there is a lack of studies of NSCs-EVs in the treatment of type 2 diabetes with stroke.

Currently, EVs-based therapy is mainly performed by intravenous injection of EVs into stroke animals, which is suboptimal for several reasons, including 1) intravenously injected EVs were found mainly accumulated in the liver, lung, and spleen, but are rarely delivered to the brain; and 2) EVs are easily lost by degradation in the circulation in vivo, due to the lack of effective protection.[12] As the recovery of brain function requires long-term sustained angiogenesis and neurogenesis, there is an urgent need to develop a novel biocompatible scaffold that can increase the retention of EVs in the lesioned brain as well as support the sustained release of EVs within the brain lesion after stroke, thus prolonging its bioactivity and accelerating neural regeneration.[12]

In this work, based on the unique microenvironment of hyperglycemia and high oxidative stress at the infarct area in stroke mice with diabetic complications, a hydrogel loaded with NSCs-EVs that is dual responsive to glucose and ROS was developed through crosslinking phenylboronic acid-modified hyaluronic acid (mHA) and commercially available Polyvinyl alcohol (PVA). The synthetic phenylboronic acid (PBA) derivatives have good glucose responsiveness and efficient ROS scavenging properties in aqueous environments. The features of PBA derivatives make them perfect candidates for glucose-regulated insulin delivery systems and are used to repair diabetic wound.[13] To the best of our knowledge, the therapeutic effect of this type of hydrogel as EVs carrier on diabetic stroke has never been studied. The resultant hydrogel was injectable and exhibited self-healing properties while prolonging the retention time and biological activity of EVs in the brain. In addition, NSCs-EVs contain key factors including miRNAs associated with angiogenesis, and can be sustained-release from the hydrogel in response to the microenvironment of ischemic brain, ultimately promoting angiogenesis in the ischemic cortical area, reducing brain atrophy volume and further improving neurobehavioral functional repair in diabetic stroke mice.

2. Results

2.1. Fabrication and Characterization of HA-PBA

As shown in **Figure 1**a, the mHA polymer was first prepared through an amidation reaction between the carboxyl group of HA backbone and amino group with the presence of DMTMM catalyst. The UV–vis spectrum of mHA showed the maximum absorption peak at 280 nm (Figure 1b), which might be related to the existence of a phenyl ring of phenylboronic acid. The 1H NMR spectroscopy shown in Figure 1c revealed the aromatic proton peaks (between 7.5 and 8.0 ppm), consistent with the typical peaks of APBA, appearing in the spectrum of mHA, which indicates that the APBA had been successfully grafted in HA. The results of fourier Transform Infrared (FT-IR) spectroscopy showed that the stretching vibration absorption peaks of a carboxylate group (1410 and 1609 cm^{-1}) and C–OH vibration (1040 cm^{-1}) appeared in both the HA and mHA samples. However, only the spectrum of mHA had the distinctive peaks at 1647 and 1350 cm^{-1}, which are corresponded to amide bond and O–B–O bend, respectively (Figure 1d). All these results demonstrated that mHA polymer was successfully prepared and could be used for further hydrogel preparation.

2.2. Fabrication and Characterization of mHA-PVA Hydrogel

Inversion assays were conducted to test the sol-to-gel transition of the designed hydrogel system. As shown in **Figure 2**a, both single mHA and PVA solutions exhibited flowing properties after inverting the tubes. In contrast, a rapid sol-to-gel transition could be observed within 30 s after mixing these two solutions at room temperature, and there was no fluidity after turning the tube upside down, indicating that the hydrogels were cross-linked quickly. The morphology of the cross-sections of the hydrogels was examined by scanning electron microscope (SEM). The SEM images demonstrated that the pore sizes in hydrogels reduced from 130 to 20 μm when the concentration of the precursor solution increased (Figure 2b). Due to the higher degree of cross-linking, which will be advantageous for nutrient penetration and cell invasion, Gel-2 (1.2% w/v) and Gel-3 (1.4% w/v) had more homogeneous in pore distribution when compared to Gel-1, (1.0% w/v). The viscoelasticity and stability of the dynamic cross-linked hydrogel were investigated by rheological tests. The curves for strain amplitude sweeps of the mHA-PVA hydrogels in Figure 2c showed that the storage modulus (G') of all three samples significantly exceeded the loss modulus (G'') in the range of linear viscoelastic domain, indicating the successful formation of a stable network in hydrogels. The storage modulus of Gel-1, Gel-2, and Gel-3 were 57.0 ± 6.7, 285.0 ± 28.3, and 1125.6 ± 132.0 pa, respectively. The storage modulus of Gel-2 hydrogel was close to that of mouse brain tissue.[1] The breakdown of the hydrogel network and the transition from gel-to-sol may be the cause of the loss modulus (G'') exceeding the storage modulus (G') when the strain exceeded 1175% for Gel-1, 802% for Gel-2, and 611% for Gel-3, respectively. Although Gel-1 hydrogel successfully gelled, its mechanical properties were far lower than that of Gel-2 and Gel-3. In addition, the values of G' of the three samples increased by 4.9 times and 18.9 times with an increase in concentrations of the precursor solution from 1.0% (w/v) to 1.2% (w/v) and 1.4% (w/v), respectively. The frequency sweep tests shown in Figure S1 (Supporting Information) revealed that G' is larger than G'' in the tested frequency range for all three mHA-PVA hydrogels, indicating that all three hydrogels maintain their elastic properties.

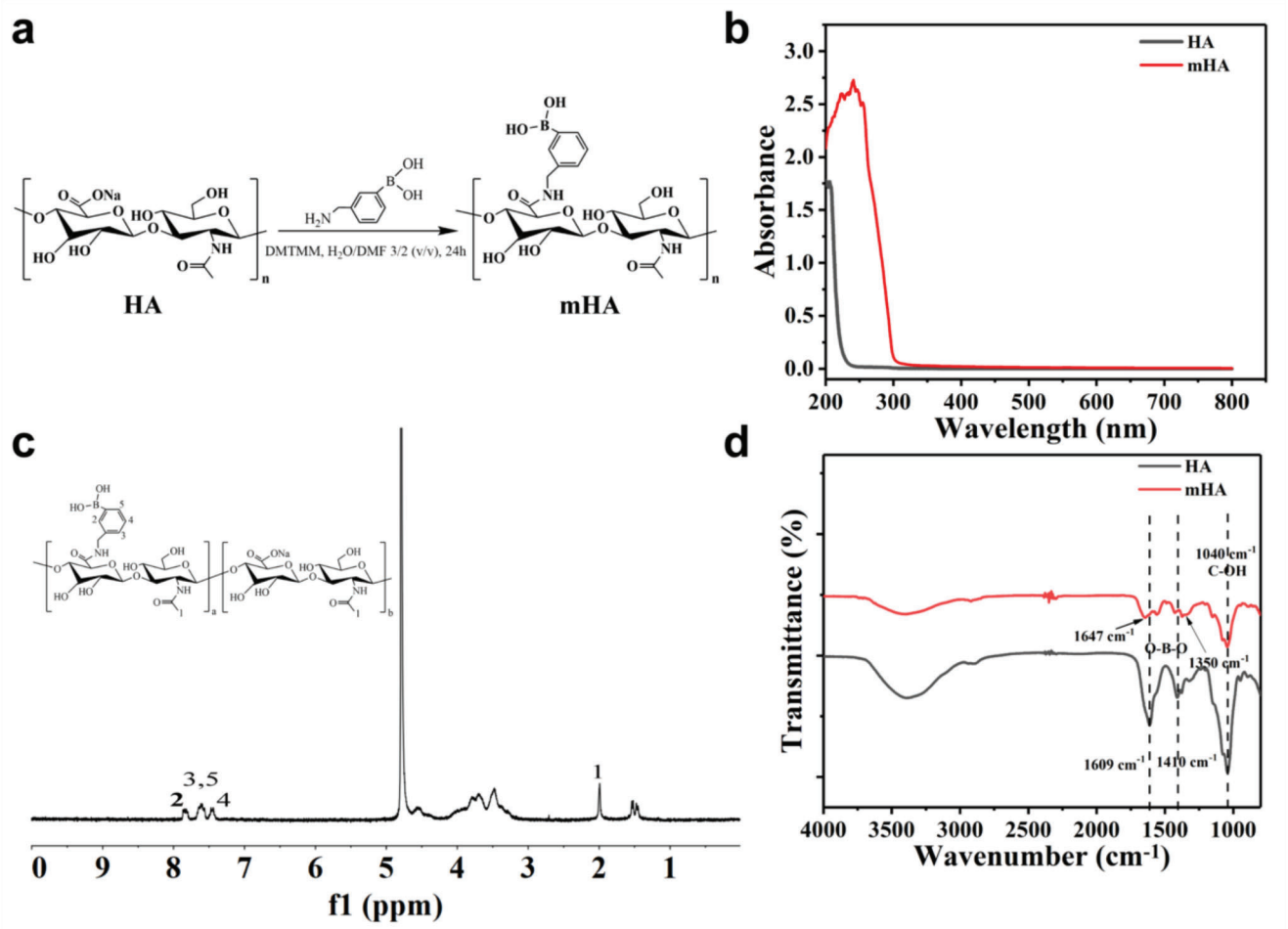

Figure 1. Fabrication and characterization of mHA. a) The synthetic route of mHA polymer. b) UV–vis spectra of HA, and mHA. c) 1H NMR (D2O) spectra of mHA. d) FTIR spectra of HA, mHA.

As shown in Figure 2d, all three hydrogels displayed a general decrease in viscosity with the increased shear rate, illustrating that mHA-PVA hydrogels exhibited shear-thinning behavior under continuous flow circumstances. The shear-thinning behavior endowed hydrogels with manipulation multiplicity, such as extrusion or injectability. It is important to note that Gel-1, Gel-2, and Gel-3 had viscosities of 198.7, 3132.6, and 9419.73 Pa.s at a shear rate of 0.1 s^{-1}; however, when the shear rate was increased to 10 s^{-1}, Gel-1 and Gel-2's viscosities dropped to 22.4 and 105.8 pa.s, respectively. Besides, Gel-3 has a viscosity of 250.3 pa.s, which is difficult to be injected compared to Gel-1 and Gel-2 (Figure 2e). As shown in Figure S2 (Supporting Information), due to the high initial viscosity of Gel-3, the needle disengaged from the syringe during the injection process, which was not conducive to injection.

The boronate ester formation and dissociation cycles could result in many notable hydrogel peculiarities, including self-healing or self-repairing. The quantitative analysis results of the self-healing capacity of hydrogels showed the modulus of Gel-1 and Gel-2 recovered to 98.5% and 98.1%, respectively, after two damage cycles, indicating that these two groups of hydrogels had good self-healing characteristics. However, the modulus of Gel-3 recovered to 87.9%, because of the high degree of cross-linking and prolonged self-healing time. The self-healing property of the hydrogels was examined by a stretching test. The results showed two semicircle hydrogels labeled with methylene blue (purple) and rhodamine B (red) were well-integrated and remained connected under a certain strain, suggesting that these hydrogels had good self-healing properties (Figure 2f). Furthermore, after two hours, the two dyes penetrated each other, and the two hydrogels fused together.

2.3. Degradation of HA-PVA Hydrogels in Response to Glucose and Reactive Oxygen Species (ROS)

The swelling behavior of hydrogels was further studied in PBS (pH 7.4) at 37 °C. As presented in Figure S3 (Supporting Information), the swelling ratio of mHA-PVA hydrogels was ranged from 16.4 g/g to 27.1 g/g with the precursor solution concentration increased from 1.0% (w/v) to 1.4% (w/v). Since the boronate ester bond has a unique response to glucose and hydrogen peroxide, the degradation of hydrogels in response to glucose and oxidative stress was measured. Previous studies showed that the

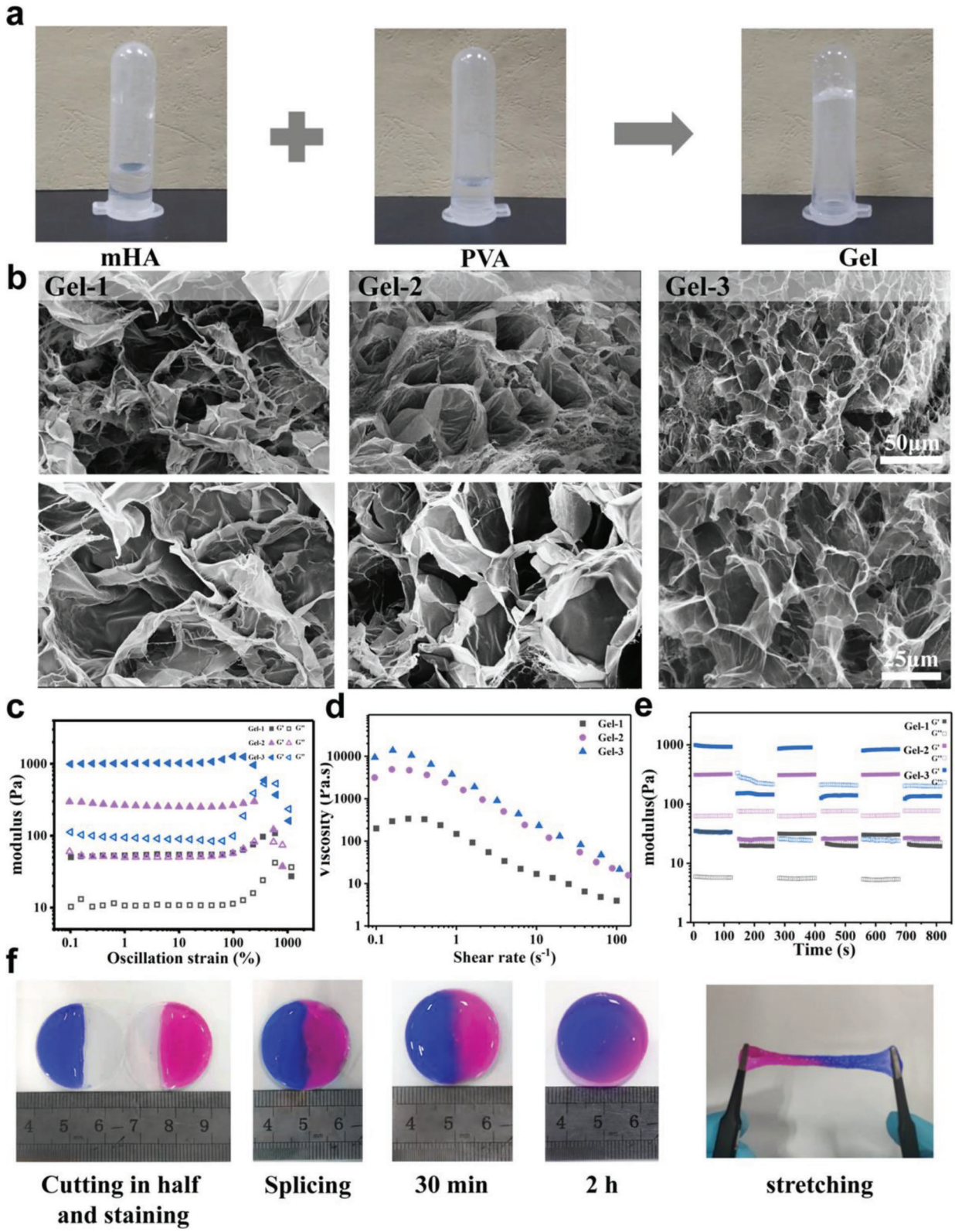

Figure 2. Characterization of mHA-PVA hydrogels. a) Photographs showed the gelation of the hydrogels. b) The morphology of hydrogel characterized by SEM. Bar = 50 or 25 μm. c) Frequency sweeps tests of Gel-1 (mHA (1.0%, w/v), PVA (1.0%, w/v)), Gel-2 (mHA (1.2%, w/v), PVA (1.2%, w/v)) and Gel-3 (mHA (1.4%, w/v), PVA (1.4%, w/v)). d) Shear rate-dependent viscosity change of Gel-1, Gel-2, and Gel-3. e) Alternate step strain sweep experiment of Gel-1, Gel-2, and Gel-3. f) Appearance of self-healing process between two different colored semicircle hydrogels.

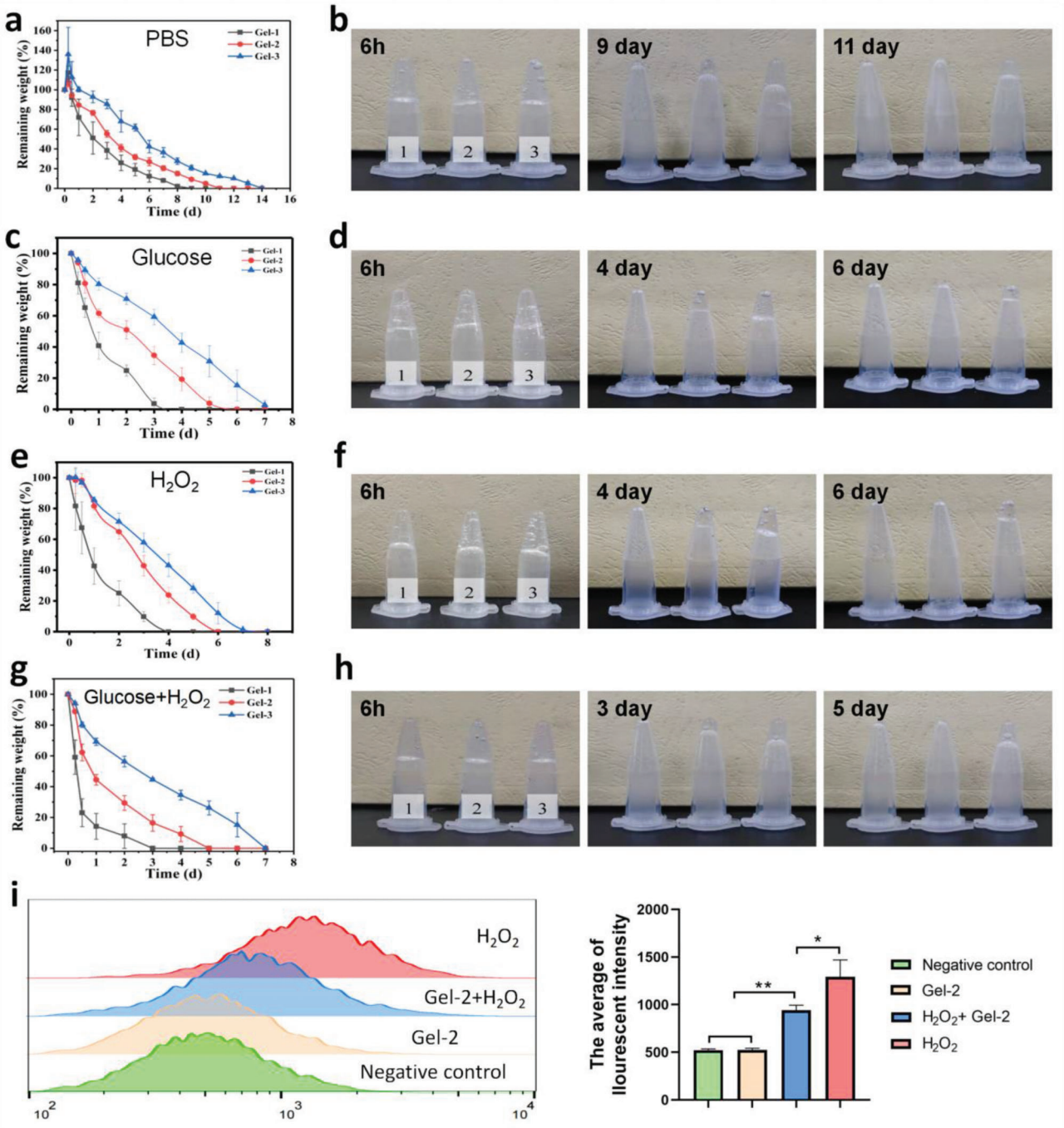

Figure 3. Characterization of the degradation of mHA-PVA hydrogel in response to glucose and ROS. a,b) Degradation profile of hydrogels in PBS. c,d) Degradation profile of hydrogels in PBS in response to glucose solution (300 mg dL^{-1}) ($n = 3$). e,f) Degradation profile of hydrogels in H_2O_2 solution (0.2 mmol) ($n = 3$). g,h) Degradation profile of hydrogels in mixed glucose and H_2O_2 solution ($n = 3$). i) Flow cytometry showed the average fluorescent intensity of DCFH-DA-HUVECs incubated with PBS, Gel-2, Gel-2 + H_2O_2, and H_2O_2 (n = 3). $^{*}p < 0.05$; $^{**}p < 0.01$.

concentration of H_2O_2 at the lesion area of the ischemic brain can reach 0.1–0.2 × 10^{-3} M, and the random plasma glucose, according to the glycemic criteria for type 2 diabetes, were set ≥ 200 mg dL^{-1}.[14] We chose 0.2 × 10^{-3} M H_2O_2 and 300 mg dL^{-1} glucose as the experimental condition due to the fact that postprandial plasma glucose would be greater and typically exceed 200 mg dL^{-1}. After the hydrogels were treated with PBS solution, Gel-1, Gel-2, and Gel-3 were almost completely degraded after 9, 11, and 14 days (**Figure 3**a,b). As illustrated in Figure 3c,d, after the hydrogels were treated with 300 mg dL^{-1} glucose solution, Gel-1, Gel-2, and Gel-3 were almost completely degraded after 4, 6, and 8 days (Figure 3c,d). Similarly, Gel-1, Gel-2, and Gel-3 treated with hydrogen peroxide were completely degraded after 4, 6, and 8 days (Figure 3e,f). The research was further conducted on degradation

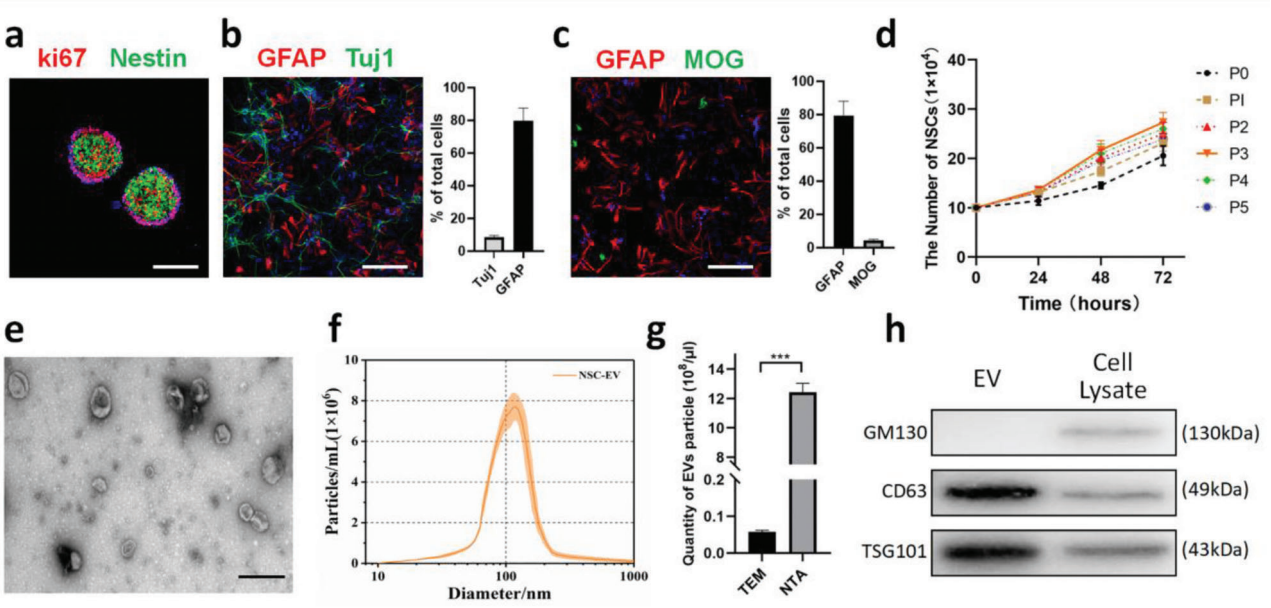

Figure 4. Characterization of NSCs and NSCs-EVs. a) Morphological characterization of NSCs and immunofluorescence staining of nestin and Ki67 in NSCs. b,c) Representative fluorescent images of NSCs differentiate into astrocytes (GFAP), neurons (Tuj1), and oligodendrocytes (MOG). Scale bar = 100 μm. d) The proliferation curve of NSCs from P0 to P5 ($n = 3$). e) Representative TEM image of NSCs-EVs. Scale bar = 500 nm. f) Size distribution of EVs based on NTA measurement ($n = 3$). g) Quantitative analyses of NSCs-EVs particle ($n = 3$). h) Membrane proteins of NSCs-EVs detected by Western blot analysis. All data are presented as the mean ± SD $^{*}p < 0.05$, $^{**}p < 0.01$, and $^{***}p < 0.001$.

time of these three groups in glucose and hydrogen peroxide mixtures. Results showed the degradation time of these three groups of hydrogels in mixed solution was shortened to 3, 5, and 7 days respectively (Figure 3g,h). Regarding the above-mentioned morphology, mechanical properties, injectability, self-healing, and responsive degradation ability, Gel-2 was chosen as the best EVs delivery vehicle for our upcoming research. In addition, we tested the degradation of Gel-2 in response to different concentrations of glucose or hydrogen peroxide solution, respectively. The results showed that the degradation of Gel-2 was both glucose and hydrogen peroxide concentration dependent (Figure S4, Supporting Information). We simulated the process of ROS scavenging in a transwell chamber to further confirm whether the hydrogel can shield cells from ROS. Gel-2 and H_2O_2 were added to the upper chamber to mimic the cellular environment, and DCFH-DA was used to measure the intracellular ROS levels. According to the flow cytometry findings, H_2O_2 supplementation in the cellular environment considerably enhanced the intracellular ROS content of HUVECs when compared to the control group, whereas the addition of Gel-2 had no significant influence on the accumulation of ROS in the cytosol. In addition, Gel-2 supplementation has the ability to significantly diminish the accumulation of ROS in cells with the existence of H_2O_2. This finding suggested that Gel-2 can act as a protective agent by consuming H_2O_2 from the environment.

2.4. Characterization of NSCs and NSCs-EV

During embryonic day 13.5, NSCs locate in the ventricular-subventricular zone. However, adult NSC populations are located in different regions along the ventricular-subventricular zone and their distinct properties are acquired during development, therefore different adult NSCs are characterized by the differential expression of specific transcription factors, which raises the possibility that they are functionally heterogeneous.[15] While one of the main features of embryonic NSCs is their high proliferative rate, the opposite is true for adult NSCs, which remain for long periods out of the cell cycle in G0.[16] In terms of cell homogeneity and extracellular vesicle yield, embryonic NSCs are better. Thus, we chose NSCs isolated from the telencephalon of the embryonic 13.5-day mice instead of adult NSCs. These NSCs were shown Nestin positive, and Ki67 was highly expressed in NSCs as a proliferating cell nuclear antigen of cells (**Figure 4**a). As well as NSCs could be differentiated into astrocytes (GFAP-positive), neurons (Tuj1-positive), and oligodendrocytes (MOG-positive) by culturing with the differentiation medium. As shown in Figure 3b,c, above 75% of NSCs differentiated into astrocytes, and a small portion of NSCs differentiated toward neurons (8.2 ± 1.5%) and oligodendrocytes (4.1 ± 1.1%). The growth curve graph and soft agar colony formation assay results showed that isolated primary NSCs still maintained the proliferation capacity after several passages, indicating that NSCs have a potential for self-renewal (Figure 4d; Figure S5, Supporting Information). Extracellular vesicles were isolated from the medium of NSCs, and characterized by TEM and nanoparticle tracking analysis (NTA). The TEM images showed cup-shaped vesicles (Figure 4e), which is consistent with the morphological characteristics of extracellular vesicles. The NTA data displayed the average diameter of EVs was 146 ± 17 nm (Figure 4f). We statistically analyzed the results of TEM and NTA, and the number of EVs particle detected by NTA was 210-fold higher than the quantification via TEM (Figure 4g), which may be attributed to the loss of EVs during the TEM samples preparation process with several times of staining and washing. Furthermore,

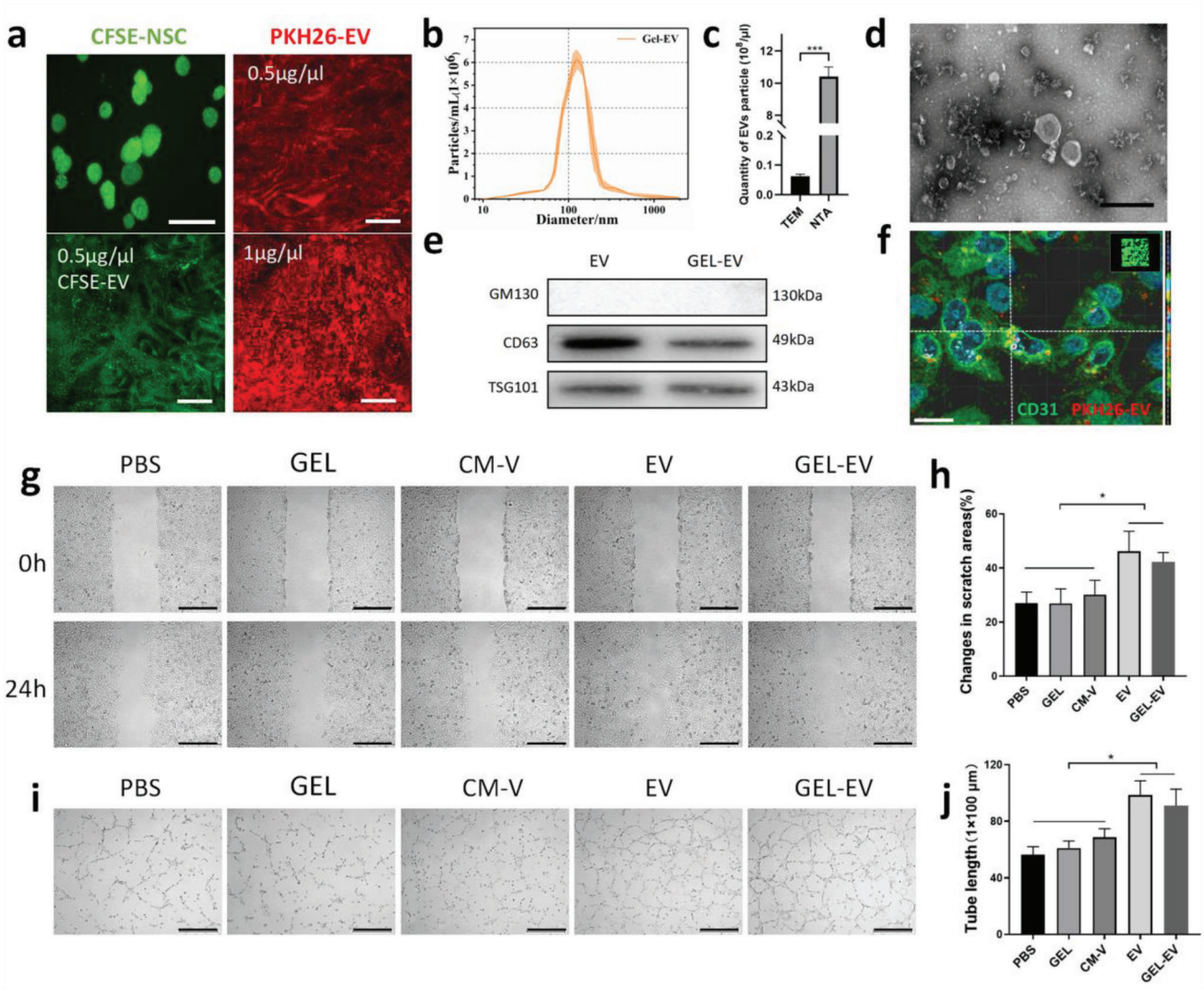

Figure 5. Gel-EVs degradation products promote the migration and tube formation of HUVECs. a) Images of CFSE-labeled NSCs (green), CFSE-labeled NSCs-EVs (green) and PKH26-labeled NSCs-EVs (red) encapsulated in Gel. Scale bar = 50 μm. b) Size distribution of NSC-EVs released from hydrogels based on NTA measurement ($n = 3$). c) Quantitative analyses of NSCs-EVs particle released from hydrogel ($n = 3$). d) Representative TEM image of NSCs-EVs released from hydrogel. Scale bar = 500 nm. e) Membrane proteins of NSCs-EVs released from hydrogels detected by Western blot analysis. f) Cellular immunofluorescence analysis revealed that PKH26-labeled NSCs-EVs (red) released from hydrogel were internalized by CD31+ HUVECs (green). Z stack and Scale bar = 20 μm. g) Representative images of scratching assay in HUVECs treated with PBS, Gel degradation products (Gel), vesicles from fresh culture medium (CM-V), NSCs-EVs (EV), and degradation products of Gel-EVs (Gel-EV). Scale bar = 500 μm. h) Quantitative analysis of the migration area of each group at 24 h in scratching assay ($n = 3$). i) Representative images of tube formation assay on matrigel in HUVECs treated with PBS, Gel, CM-V, EV, and Gel-EV. Scale bar = 500 μm. j) Quantitative analyses of the tube length in tube formation assay ($n = 3$). All data are presented as the mean ± SD. $^{*}p < 0.05$, $^{**}p < 0.01$, and $^{***}p < 0.001$.

the western blot results showed the EVs markers such as CD 63 and TSG 101 were expressed in NSCs-EVs, and there was no expression of the negative marker protein GM130 (Figure 4h). All the above results demonstrated that we had successfully isolated EVs from NSCs.

2.5. Gel Reserved the Bioactivity of EVs After Encapsulation

NSCs-EVs were isolated from CFSE (Carboxyfluorescein Succinimidyl amino Ester) labeled NSCs to test whether we successfully load EVs into Gel. Besides, in another set of experiment, PHK26 was also used to directly label NSCs-EVs. Then the labeled NSCs-EVs were mixed with Gels. Confocal images indicated that labeled EVs exhibited a well-monodispersed distribution in the hydrogels, and the fluorescence signals in the hydrogels increased as EVs concentration increased (**Figure 5**a). To confirm the bioactivity of NSCs-EVs released from the hydrogels, the Gel-EVs were immersed in high-glucose DMEM (glucose concentration: 450 mg dL^{-1}) for 24 h for degradation. The release curves of EVs from hydrogels in DMEM medium are shown in Figure S6 (Supporting Information). The NTA data

displayed the average diameter of EVs released from hydrogels was 159 ± 31 nm (Figure 5b). TEM image revealed that the EVs released from hydrogels exhibited an intact vesicle structure (Figure 5d). We performed a statistical analysis of the results of TEM and NTA, and the amount of EVs particles detected by TEM was 0.6% of that quantified by NTA (Figure 5c). As the EVs would be lost a lot during the TEM samples preparation process with several times of staining and washing, the number of EVs particles quantified by TEM was lower than that by NTA. Hence, in this study, we determined the total protein amount of EVs detected via BCA assay as the administration dosage in this study. The western blot results showed the EVs markers such as CD 63 and TSG 101 were expressed in Gel-EVs, and there was no expression of the negative marker protein GM 130 (Figure 5e). And the released EVs from hydrogels were uptake by the HUVECs after 12 h co-culture (Figure 5f). To further explore the bioactivity of EVs released from hydrogel, the scratching assay and tube formation assay were performed. Besides, in order to exclude the interference of vesicles that existed in fresh NSCs culture medium (CM-V), we also performed same experiments using culture medium. Results showed that direct supplement of EV and supplement of Gel-EVs significantly increased migration of HUVECs (Figure 5g,h). To further confirm the effects of NSCs-EVs on angiogenesis, tube formation assay was performed. Six hours of EVs or Gel-EVs treatment increased tube formation of HUVECs without influencing the cell viability (Figure 5i; Figure S7, Supporting Information). Quantitative analysis showed that treatment with EVs or Gel-EVs remarkably increased the total tube length of HUVECs than PBS, Gel, and CM-Vs treatment (Figure 5j). It is also noted that adding NSCs-EVs released from Gel hydrogel achieved comparable effect on tube formation and migration of HUVECs, suggesting Gel hydrogel is EV-friendly and could well maintain the bioactivity of EVs. However, addition of Gel hydrogel degradation products or vesicles from fresh NSCs medium into HUVECs did not affect their function. These results demonstrated that NSCs-EVs encapsulated within hydrogels remained bioactivity and the capability of facilitating angiogenesis.

2.6. Gel Increased NSCs-EVs Retention and Sustained NSCs-EVs Releasing in Response to Glucose and ROS

To further investigate the degradation of Gel-EVs in response to ROS and glucose, Gel-EVs were treated with different concentration of H_2O_2, or glucose, or H_2O_2 + glucose. Non-glucose and non-ROS responsive CCS-HA-CHO hydrogel loaded with EVs (CG-EVs) was used as control. The released curves showed that Gel-EVs (Gel-EV) achieved sustained release of the EVs in response to both glucose and hydrogen peroxide, and the release rate of EVs from hydrogel was glucose and hydrogen peroxide concentration dependent (**Figure 6**a–c). This is due to the fact that the boronate ester bonds have specific responses to glucose and hydrogen peroxide.[17] The release rate of CG-EVs was substantially slower than that of Gel-EVs treated with glucose and hydrogen peroxide and was similar to that of PBS treatment (Figure 6d; Figure S8, Supporting Information). This phenomenon indicated that CG-EVs were not responsive to glucose and hydrogen peroxide. Then, we investigated the retention of DIR-labeled EVs after injection in diabetic stroke mice brain. Non-glucose/ROS responsive CG-EVs group and DIR group were used as controls, respectively. We found that injection of EVs encapsulated within the Gel hydrogel resulted in better retention in the brain and prolonged the release time of EVs, compared to EV only group (Figure 6e,f), indicating our Gel controls the local sustained release of EVs at the site of infarct area by acting as a reservoir of EVs, and the appropriate micromorphology and pore structure of hydrogel ensure that it has sufficient internal space to load and encapsulate the EVs. In addition, injection of CG-EV achieved the longest retention time, due to the low degradation capacity of CG hydrogel. It should be noted that injection of DIR alone achieved most persistent signals. DIR is a class of lipophilic fluorescent dyes, and is able to directly label cell membranes and hydrophobic tissues after injection, thus injection of DIR alone exhibits long retention in vivo as endogenous cells could uptake DIR. One of the challenges of DIR labeled EVs is that DIR dye may diffuse to neighboring cells, causing non-specific signal. However, lipophilic dyes labeling is still the most commonly used and convenient strategy for tracking EVs. Other strategies such as nuclear imaging and MRI could be used for EVs tracking in future study.

2.7. Injection of Gel-EVs Reduced Brain Atrophy Volume and Promoted Neurobehavioral Recovery After Stroke via Increasing Angiogenesis

In order to examine the treatment effect of Gel-EVs on stroke, brain atrophy volume and neurobehavioral recovery were assessed at 14 days and 21 days after stroke. The results showed that treatment with Gel-EVs and EVs significantly reduced the brain atrophy volume at 14 and 21 days after stroke, compared to PBS, Gel, CM-V, and CG-EVs group (**Figure 7**a,c). Besides, Gel-EVs showed more efficiency than EVs alone of EVs delivery in reducing brain atrophy volume (Figure 7b,d). The neurobehavioral results showed that Gel-EV and EV treatment significantly improved sensorimotor function of mice at 14 and 21 days after stroke, compared to PBS, Gel, CM-V, and CG-EV group (Figure 7e,f), while Gel-EV treatment showed better effects in reducing the time that mice used to remove adhesive tape in the right limb during adhesive removal test, as well as decreasing the frequency of errors in the right limb during grid walking test than EVs treatment (Figure 7e,f).

Angiogenesis has been shown to occur at the ischemic core and peripheral borders as early as 4 days after cerebral ischemia,[18] and continues to increase 14 days after stroke, which is the chronic stage of stroke. Besides, angiogenesis is critical for axonal outgrowth and neurobehavioral recovery, and typically occurs 14 days after ischemia. Therefore, we started to examine angiogenesis 14 days after stroke. The results demonstrated that Gel-EV and EVs significantly increased the number of blood vessels (Figure 7g–j). In our study, we observed improved neurobehavioral recovery in Gel-EV group than those in EVs-only group in sticky tape test and grid walking test, and considering that the hydrogel treatment alone did not significantly reduce the brain atrophy volume and improve neurobehavioral recovery, suggesting the hydrogel we designed in our study did not facilitate therapeutic effect for stroke. Thus, we can conclude that the

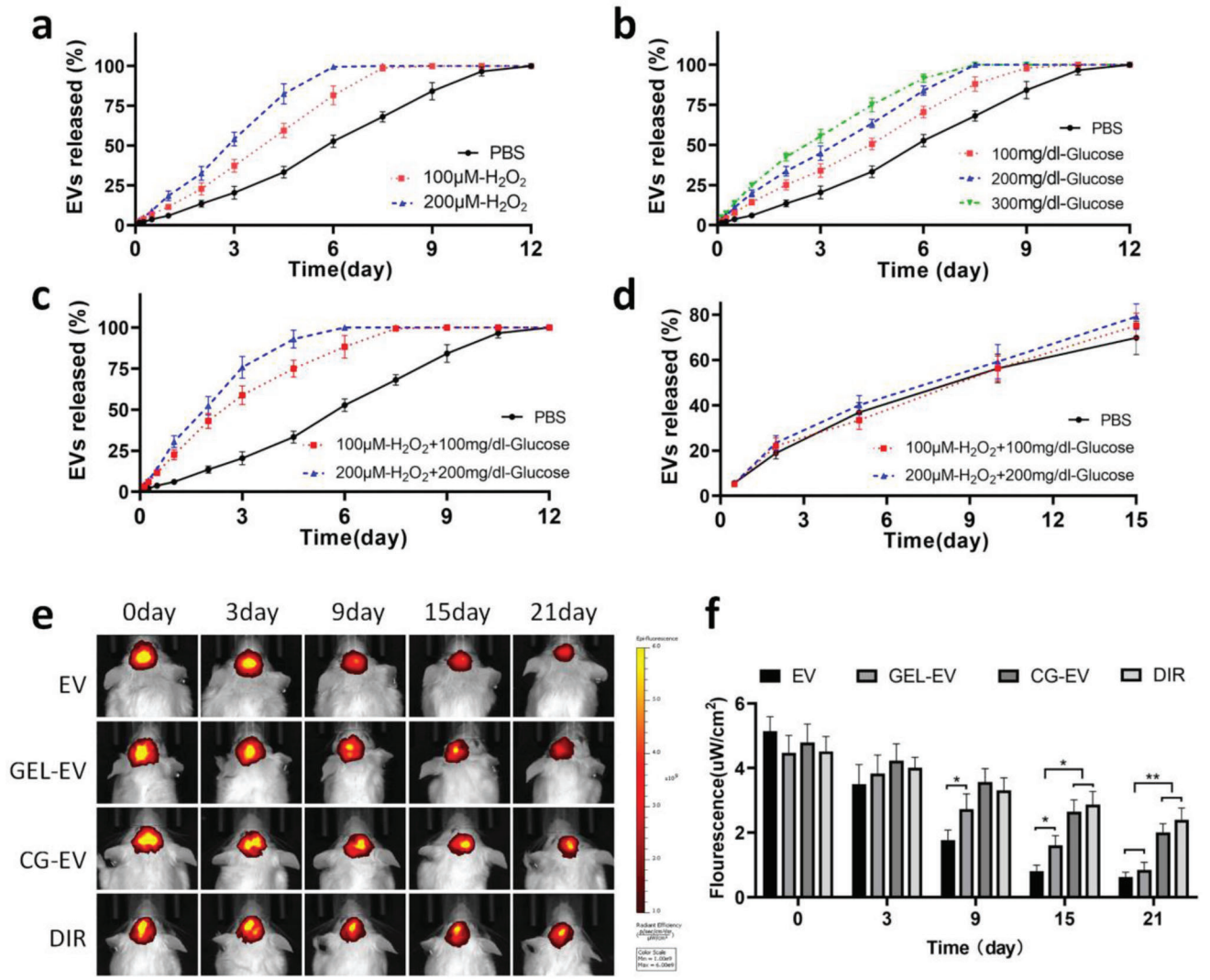

Figure 6. The release curves of NSCs-EVs from Gel-EVs in vitro and in vivo. a–c) Release curves of EVs from Gel-EVs responding to different concentrations of glucose and hydrogen peroxide ($n = 3$). d) Release curves of EVs from CG-EVs responding to different concentrations of glucose and hydrogen peroxide ($n = 3$). e) Fluorescence images of mice after injection of DiR-labelled EVs, Gel-EV, CG-EV, and DIR. f) The quantitative analysis of fluorescence intensity ($n = 6$). All data are presented as the mean ± SD $^{*}p < 0.05$, $^{**}p < 0.01$, and $^{***}p < 0.001$.

hydrogel-mediated sustained release of EVs was a crucial factor to further improve the therapeutic effect of EVs.

2.8. Angiogenic Related MiRNAs were Enriched in NSCs-EVs

To further identify the mechanism of why injection of Gel-EV increased angiogenesis after stroke, we analyzed the miRNAs targeting the angiogenesis-related signaling pathways in NSCs-EVs. We performed miRNA sequencing of NSCs-EVs, and used EVs from fibroblast (Fibroblast-EVs) as a control. In sequencing, we identified 227 differentially expressed miRNAs, of which 117 miRNAs were significantly upregulated, including pro-angiomiRs. miRNAs derived from NSCs-EVs were ranked according to average read counts of three samples (highest to lowest). Total reads of the top 20 miRNAs were shown in **Figure 8**a, and the top 8 miRNAs accounted for 77.4% of total miRNAs present in NSCs-EVs (Figure 8b). Angiogenesis is known to be regulated by several regulators and signaling molecules, including vascular endothelial growth factor (VEGF), fibroblast growth factor (FGF), and epidermal growth factor (EGF) signaling pathway.[19] The VEGF signaling pathway (KEGG 0 4370) related miRNAs were predicted by DIANA Tools and analyzed in three methods (Tarbase, microT, and Targetscan). The number of predicted miRNAs related to VEGF signaling pathway in Tarbase, microT, and Targetscan was 202, 919, and 593, respectively. Then the intersection of these three datasets was obtained by Venn, showing 90 miRNAs were related to VEGF signaling pathway with a higher confidence (Figure 8c). Matching these 90 miRNAs with top eight miRNAs, we found that five out of eight miRNAs were contained in the VEGF-related miRNAs dataset including miR-9-5p, let-7f-5p, let-7i-5p, let-7c-5p, and let-7g-5p. These

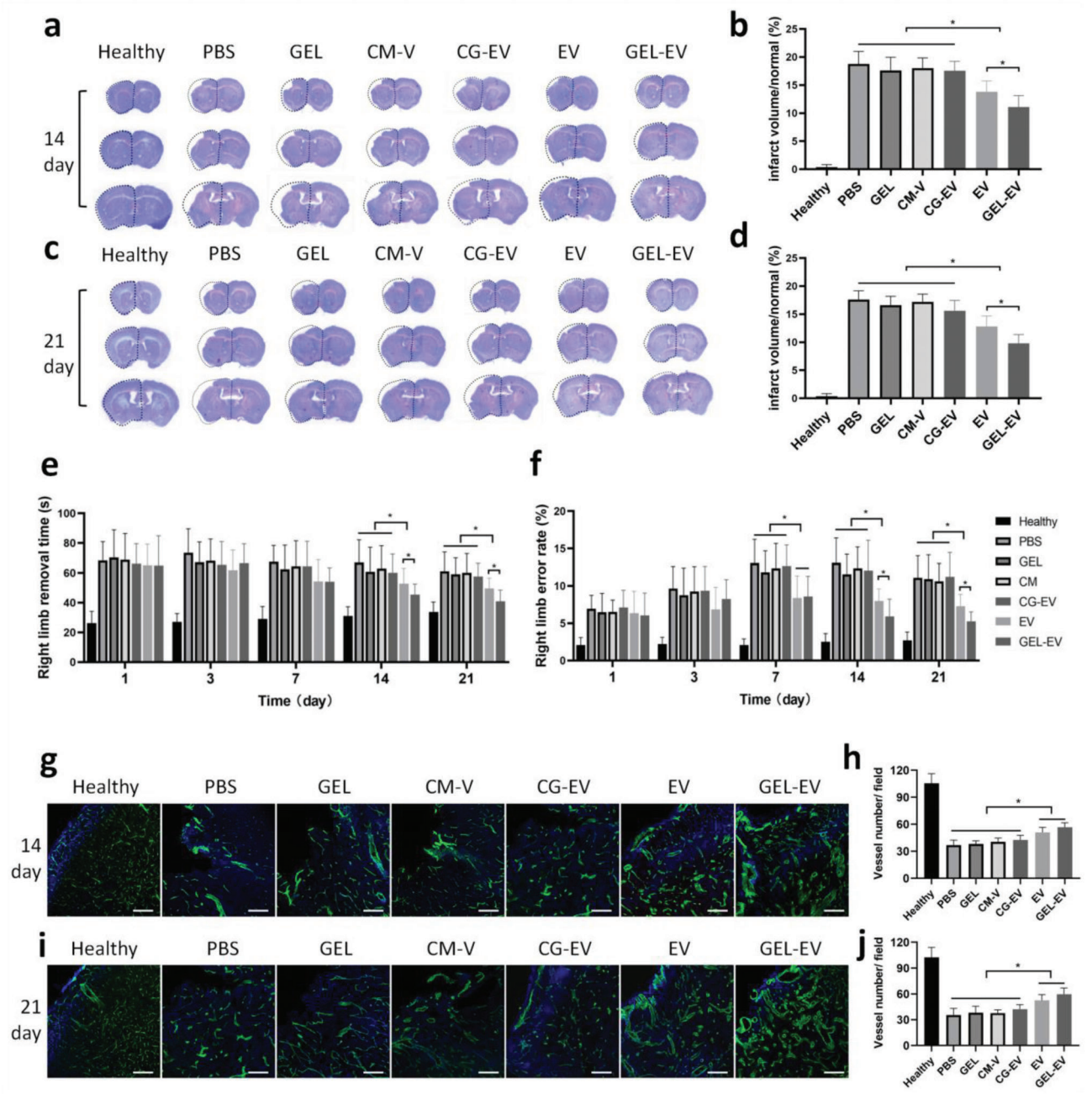

Figure 7. Injection of Gel-EVs reduced brain atrophy volume and improved angiogenesis in ischemic mice. a,c) Representative photomicrographs of coronal sections stained by cresyl violet for evaluation and quantification of the brain atrophy volume in each group treated with PBS, Gel, CM-V, CG-EV, EVs, and Gel-EV after 14 and 21 days of ischemic stroke. b,d) Bar graph showed the percentage of infarct volume normalized to the contralateral side ($n = 6$). e,f) Sensorimotor function test showed the neurobehavioral tests of mice treated with PBS, Gel, CM-V, CG-EV, EV, and Gel-EV. ($n = 9$). g–j) Immunofluorescence and quantification of CD31+ microvessels in the ipsilateral cortex after stroke in PBS, Gel, CM-V, CG-EV, EV, and Gel-EV groups at 14 and 21 days after stroke ($n = 6$). Scale bar = 150 μm. All data are presented as the mean ± SD $^{*}p < 0.05$, $^{**}p < 0.01$, and $^{***}p < 0.001$.

miRNAs were also identified as pro-angiogenic miRNAs in previous study.[20] To compare the differences in angiogenic capacity between NSCs-EVs and Fibroblast-EVs, we analyzed the expression of 5 miRNAs listed above, and previously proved pro- or anti-angiogenic miRNAs in the two groups. The heatmap showed that the most proangiogenic miRNAs listed were higher expressed in NSCs-EVs compared to Fibroblast-EVs (Figure 8d).

3. Discussion

Previous studies have demonstrated that NSCs-EVs can improve neurological outcomes of ischemic stroke models in mouse and porcine.[21] However, the efficacy of the treatment is greatly limited due to the lack of appropriate carrier to protect and extend the retention time of EVs at the lesion site, and it also failed to

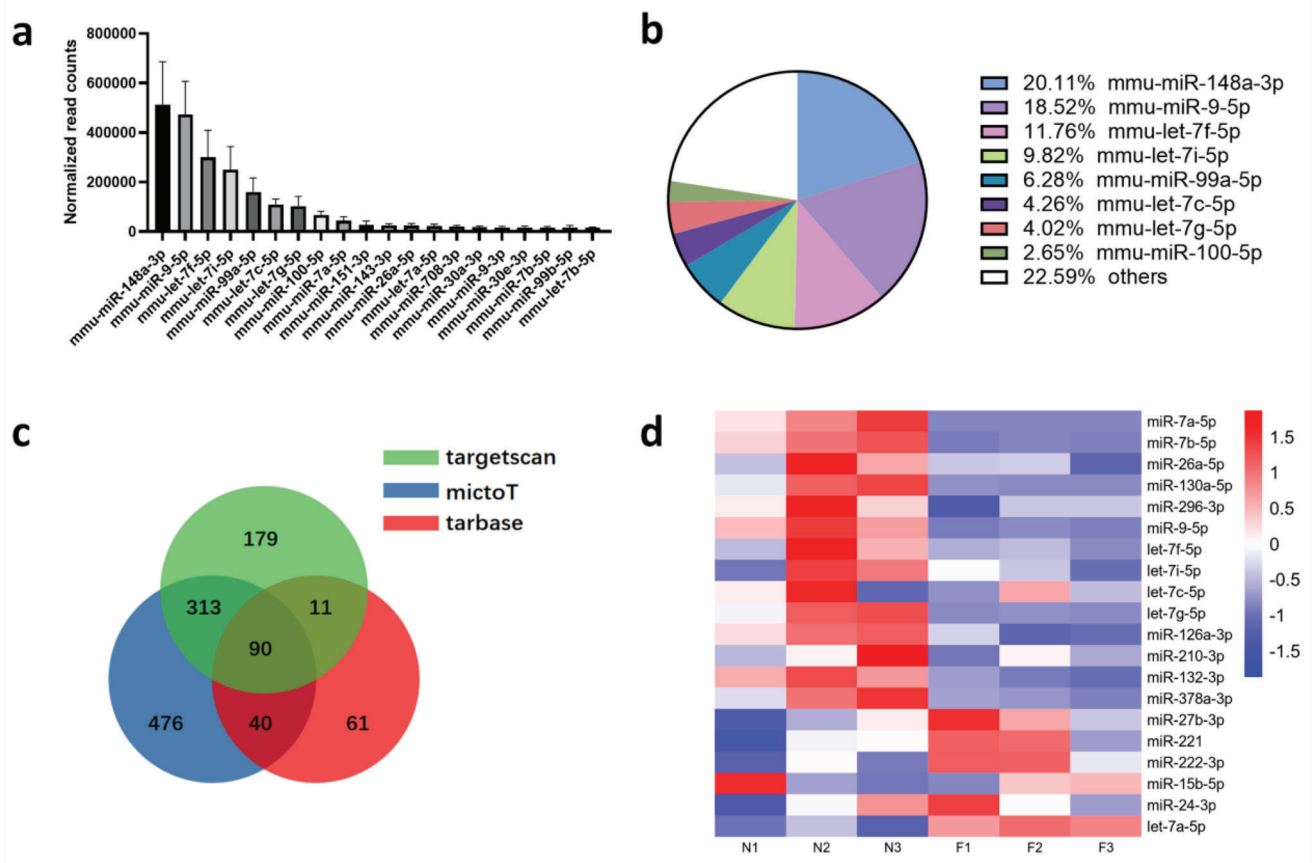

Figure 8. Angiogenic related miRNAs were enriched in NSCs-EVs. a) Total reads of the top 20 miRNAs. b) The top 8 miRNAs account for 77.4% of total miRNAs present in NSCs-EVs. c) The VEGF signaling pathway related miRNAs were predicted by DIANA Tools and analyzed in three methods (Tarbase, microT, and Targetscan). The intersection of Venn was 90 miRNAs related to VEGF signaling pathway. d) The expression heatmap of proangiogenic and antiangiogenic miRNAs were compared between NSCs-EVs with Fibroblast-EVs. N means NSCs-EVs, F means Fibroblast-EVs ($n = 3$). All data are presented as the mean ± SD $^{*}p < 0.05$, $^{**}p < 0.01$, and $^{***}p < 0.001$.

achieve long-term effective treatment. To address this challenge, we developed an injectable HA hydrogel by cross-linking mHA and PVA. This hydrogel for delivering EVs into stroke brain has several advantages: 1) Injectable, biodegradable and biocompatible; 2) EVs can be heavily loaded, and their biological activity can be protected by biomaterials; 3) Ensuring effective retention of EVs and allowing sustained release of EVs in the brain cavity; 4) Seamless hydrogel-brain integration that enables brain cells to migrate and infiltrate into the scaffold to uptake EVs. We explored the intricate and dynamic pathophysiology of stroke, concentrated on beneficial effects of this injectable hydrogels loaded with EVs on neural tissue engineering, and revealed the underlying mechanism of these biomaterials in the management of diabetic stroke. It has been demonstrated that hyaluronic acid is extremely biocompatible and supportive for a variety of tissues, and it has been developed for numerous hydrogel systems.[22] PVA is biocompatible hydrogel substance that works well for both medication delivery and tissue engineering.[23] Our hydrogel is more biocompatible with brain tissue because the extracellular matrix of the brain is distinct from other extracellular matrixes in that it is mostly made up of hyaluronic acid and proteoglycans.[24] In addition, the low elastic and shear modulus of brain tissue makes injection transplantation of the brain required. Our hydrogel exhibits self-healing properties due to BA grafted HA and may create dynamic boronate ester linkages when combined with PVA solution.[25] Based on the physical properties of this viscosity declining at high shear stress, our dynamic hydrogel enables minimally invasive grafting by fine needle injection.[26] Direct delivery of EVs to the intended injection site prevents the development of stress-induced cracks, which can increase their stability during implantation and boost the therapeutic effectiveness.[27] The injectable hydrogels can efficiently repair the extracellular matrix of the lesion cavity after being injected into the infarcted lesion area, simulating cerebral soft tissue and preventing additional harm during implantation operations.[28]

Ischemic stroke causes neuron death and tissue loss, ultimately resulting in brain cavity formation. Thus, in situ injected EVs could easily diffuse away due to the lack of structural support in the brain cavity. Hydrogel materials have been widely used as delivery tools for tissue regeneration due to their unique features, such as high-water content, injectability, biocompatibility, etc.[29] Embedding EVs in hydrogel has proven to be a feasible strategy to effectively retain EVs in situ.[30] For example, hydrogel-incorporated mesenchymal stem cell-derived EVs exhibited high

retention rate and stability, and further enhanced therapeutic effects for hindlimb ischemia and myocardial infarction.[31] Our hydrogel controls the local sustained release of EVs at the site of infarct area by acting as a reservoir of EVs, and the appropriate micromorphology and pore structure of hydrogel ensure that it has sufficient internal space to load and encapsulate the EVs. The Gel designed in our study not only increases the retention and bioactivity of NSCs-EVs in the brain, but also controls the release of NSCs-EVs in response to the microenvironment of the stroke brain, which may contribute to long-term neurobehavioral recovery. Besides that, another advantage of our hydrogel is the innate anti-oxidative property because boronate ester bond in oxidative cracking under hydrogen peroxide environment produces phenolic products and boric acid, which reduces the level of hydrogen peroxide. Previous studies have shown that H_2O_2 concentration at the lesion core area of ischemic brain can reach 0.1–0.2 × 10^{-3} M, and high ROS microenvironment remains an adverse factor to reduce the bioactivity of many neurotrophic substances, including EVs.[14a,32] Thus, it is plausible that reducing the level of ROS in brain could improve the bioactivity and retention of NSCs-EVs after injection into ischemic mice brain. It is known that EVs have to be uptake by target cell to exert their function. Even though our study showed that CG hydrogel showed better EVs retention than Gel, it is not conducive to EVs release. Thus, CG hydrogel is not appropriate for EVs-based therapy in our study.

To explore the effect of EVs-hydrogel on stroke outcome, sensorimotor function was evaluated. Results showed that Gel hydrogel loaded with NSCs-EVs significantly alleviated the ischemia-induced subcortical damage, which controlled the sensorimotor behavior. Meanwhile, the improved functional results in GEL-EVs group were better than those in EVs-only group in sticky tape test and grid walking test. In addition, difference between GEL-EVs group and EVs group in the motor function test increased over time, and considering that the hydrogel treatment alone was not significantly different from the PBS group, the hydrogel-mediated sustained release of EVs was a crucial factor to further improve the therapeutic effect of EVs. Existing studies have demonstrated that the therapeutic efficacy of EVs on brain injury is dose-dependent.[33] Because CG-EV is unable to be efficiently degraded, very few EVs can be uptake by target cell. Therefore, despite CG-EV showed long time retention in the brain, they showed negligible therapy. Consistent with previous reports,[10] EVs treatment improved performance of motor behavior in our mice model, which may be due to increased angiogenesis. The major cause of disability and death due to ischemic stroke is vascular damage, resulting in reduced blood supply that limits the delivery of oxygen, absorption of nutrients, and removal of metabolic waste products. After stroke, normoglycemic animals are able to initiate reparative neovascularization in ischemic hemispheres, whereas diabetic animals develop vascular regression, accompanied by poor functional outcome.[34] Stimulation of angiogenesis and vasculogenesis is critical for stroke recovery, not only for the improvement of cerebral blood flow and blood-brain barrier integrity but also for the enhancement of neurogenesis and neuroplasticity in the angiogenic microenvironment.[35] Inspired by this pathological occurrence, researchers have favored enhanced angiogenesis as a strategy for the treatment of ischemic stroke. EVs are small in diameter and can be transported across membranes to deliver proteins and microRNAs for angiogenesis to regulate signal transduction in an autocrine and paracrine manners under ischemic conditions.[36]

To further identify the mechanism of NSCs-EVs increased angiogenesis after stroke, we analyzed the miRNAs targeting the angiogenesis related signaling pathways in NSCs-EVs, and fibroblast-EVs were used as control. miRNAs including miR-378, miR-126, let-7f were reported to regulate the response of the vascular endothelium to angiogenic stimuli,[37] and they are differentially expressed between NSCs-EVs and Fibroblast-EVs. These pro-angiomiRs can be divided into two categories based on their mechanisms, one of which is to target endothelial cell sprouting, migration, and tubulogenesis, such as let-7 family.[38] ALK5 as an important modulator of angiogenesis, is a target of let-7f. Treatment with let-7f mimic or let-7f overexpression reduced the expression of ALK5, SMAD2/3, and PAI-1 both in vitro and in vivo, rescuing angiogenesis in HUVECs exposed to detrimental conditions.[39] The other category is to target VEGF signaling pathway, such as miRNA-126, and miRNA-378. miRNA-126 is mainly expressed in endothelial cells, and its expression is significantly reduced in the serum and ischemic brain tissue of type 2 DM stroke mice compared with non-DM stroke mice.[40] Umbilical cord blood cells (UCBCs) treatment significantly increased miRNA-126 expression in ischemic brain tissue and significantly improved vessel density of diabetic stroke mice, while knockdown of miRNA-126 expression in UCBCs dramatically attenuated the therapeutic effect of HUCBCs, indicating that miRNA-126 substantially contributes to therapeutic effects in DM stroke.[40] During angiogenesis, endothelial cells had to be activated first in response to various cytokines and chemokines such as VEGF-A, bFGF. Low expression of miRNA-126 was able to directly reduce VEGF-A-mediated ERK and AKT phosphorylation levels. Additionally, previous study suggested that miRNA-378 regulated VEGF-A by inhibiting fused-enhanced cell survival and enhanced angiogenesis.[37,41] In addition, we believed that the NSCs-EVs may exert pro-angiogenic effects on endothelial cell by mediating protein delivery through cell membrane fusion with recipient cells. A study comparing angiogenesis-related protein content in NSCs-EVs and NSCs found that NSCs-EVs had the highest VEGF-A content among angiogenesis-related proteins and VEGF-A has been more enriched in NSCs-EVs compared to NSCs. Down-regulation of VEGF-A expression in EVs inhibits the migration, proliferation, and tube formation ability of endothelial cells in co-culture systems.[42] In summary, our study revealed that pro-angiomiRs and VEGF-A mediate the activation of VEGF signaling pathway, which might be a potential mechanism by which NSCs-EVs promote angiogenesis in diabetic stroke mice.

4. Experimental Section

Synthesis and Characterization of Phenylboronic Acid Modified HA (mHA): The mHA derivative was prepared in an aqueous solution by an amide coupling reaction between APBA and HA. To this end, APBA (0.034 g, 0.25 mmol) was added to 20 mL of water/DMF (3/2, v/v) mixture containing DMTMM (0.090 g, 0.33 mmol) and HA (0.100 g, 0.25 mmol). The pH of the solution was adjusted to 6.5 using 0.5 M aqueous NaOH. The solution was then stirred for 24 h, and the mHA was purified by ultrafiltration using deionized water for 5 days and the products were recovered

by freeze-drying. 1H NMR spectra of the mHA samples were recorded by applying a 90° tip angle for the excitation pulse, and a 10 s recycle delay for accurate integration of the proton signals. The modification ratio of the phenylboronic acid group was measured by the ratio of the integral of aromatic protons from the conjugated phenylboronic acid group to the integral of the HA methyl proton peak. The Fourier transformation infrared (FTIR) spectroscopy was used to analyze the physicochemical structure of HA and mHA. Briefly, the FTIR spectra of samples in the range of 4000 to 800 cm^{-1} were obtained by attenuated total reflection FTIR (ATR-FTIR) method at a scan resolution of 4 cm^{-1}.

Preparation of the CCS-HA-CHO hydrogels: HA-CHO was prepared using periodate oxidation method. Briefly, 400 mg (1 mmol) HA was dissolved in 50 mL distilled, then 320 mg NaIO4 in 5 mL distilled water was dropwise added, respectively, and stirred for 4 h in the dark at room temperature. Next, 500 µL of ethylene glycol was added to quench the unreacted NaIO4. The solution was then stirred for another 2 h, and the mixture was exhaustively dialyzed (Mw cutoff 8000–14000) against distilled water for 5 days. HA-CHO solution (1.2% (w/v)) was prepared in PBS (pH 7.4) and mixed with an equal volume of chitosan quaternary ammonium salt solution (2%, w/v). The prepared hydrogel was labeled as HA-CCS.

Preparation and Characterization of Glucose/ROS Dual-Responsive Injectable mHA-PVA Hydrogels: The lyophilized mHA and commercially available PVA were separately solubilized in deionized water, and the pH was adjusted to 7.4 with 0.5 M aqueous NaOH. The hydrogels were prepared by mixing mHA and PVA solutions with a volume ratio of 2:1 (mHA/PVA) at room temperature, and were labeled as Gel-1 (mHA (1.0%, w/v), PVA (1.0%, w/v)), Gel-2 (mHA (1.2%, w/v), PVA (1.2%, w/v)), and Gel-3 (mHA (1.4%, w/v), PVA (1.4%, w/v)). The lyophilized hydrogel was quenched in liquid nitrogen, sprayed with gold by ion sputtering apparatus, and then the morphology was observed with S-4800 scanning electron microscope (Hitachi, Chiyoda-ku, Tokyo, Japan). The rheological properties of the hydrogel including the storage modulus (G'), loss modulus (G''), and viscosity under different conditions (frequency, oscillation strain, and shear rate) were analyzed by using the TA rheometer (DHR-2) (New castle, DE). The hydrogel samples were placed between parallel plates with a diameter of 10 mm and a gap of 1 mm. The elastic modulus (G') and viscosity modulus (G'') were measured at 37 °C by a frequency sweep between 0.1 and 100 Hz, at a strain of 10%, and a strain sweep between 0.1 and 1200%. The injectability of the hydrogels was verified by a shear rate scan between 0.1 and 100 s^{-1}. The self-healing properties of the hydrogels were investigated by monitoring the changes of G' and G'' under continuous train sweep with an alternative large oscillation force (1200%) and a small one (10%). Besides, a stretching test was also conducted to evaluate the self-healing properties of the hydrogels. Hydrogel was cut in half and stained by rhodamine B and methyl blue, respectively. Then, the two hydrogel disks were put together for 2 h to observe the self-healing process and stretch the self-healing hydrogel to observe the changes in the joints. The swelling ratio measurement of freeze-dried hydrogel were carried out gravimetrically. The weighed freeze-dried hydrogels (W_0) were immersed in the phosphate buffered saline and placed in a constant temperature shaker at 80 rpm, 37 °C. At specific intervals of time, the swollen samples were taken out and weighted (W_1). All experiments were carried out in triplicate. The swelling ratio was calculated using the following equation:

$$\text{Swelling ratio } (\%) = (W1 - W0)\,/W0 \times 100\% \quad (1)$$

In Vitro Degradation of mHA-PVA Hydrogels under Glucose and H_2O_2 treatment: Lyophilized hydrogels were weighed (M_0) and immersed in PBS solutions with different concentrations of glucose (0, 100, 300 µg dL^{-1}), At specific intervals of time, the hydrogels were taken out and lyophilized and weighed (Mt). All experiments were carried out in triplicate. The degradation ratio was calculated using the following equation:

$$\text{Remaining weight } (\%) = Mt/M_0 \times 100\% \quad (2)$$

The experiments were conducted under the same conditions except for the different concentration of H2O2 in the PBS (0, 0.1, 0.2×10^{-3} M).

Intracellular ROS Detection: Approximately 1×10^5 HUVECs were seeded in the lower chamber of the transwell. After two hours 40 µl of Gel-2 and 10 µl of H_2O_2 (1×10^{-3} M) were added to the upper chamber of the transwell. The H_2O_2 group only added 10 µl H_2O_2 (1×10^{-3} M L^{-1}) without Gel-2. After 4 h, the culture medium was discarded and a serum-free medium containing 10×10^{-6} M DCFH-DA was added to the chambers. After 20 min of incubation, the cell was washed with PBS twice and collected for flow cytometry analysis.

Isolation, Culture, and Identification of NSCs: Animal protocols were approved by the Institutional Animal Care and Use Committee (IACUC) of Med-X research institute, Shanghai Jiao Tong University, Shanghai, China (#2 019 052) and animal work in this study was performed in accordance with ARRIVE guidelines. NSCs were isolated from cerebral cortex of embryonic 13.5 d fetal mice as previously described.[43] Then, NSCs were cultured in Dulbecco's modified Eagle's medium (DMEM)/Ham's F-12 medium (Gibco, Waltham, MA) supplemented with B27 (Gibco), GlutaMAX (Gibco), 20 ng mL^{-1} epidermal growth factor (EGF; Invitrogen, Carlsbad, CA) and 10 ng mL^{-1} basic fibroblast growth factor (bFGF; Invitrogen) at 37 °C in an incubator with 5% CO_2. After culturing for 5 days, the neurospheres were centrifuged and plated in a poly-D-lysine-coated coverslip and the medium was replaced with Dulbecco's modified Eagle's medium (DMEM, Gibco) supplemented with B27, GlutaMAX and 10% fetal bovine serum (FBS, Gibco, USA). DMEM containing 2% FBS was used to induce cell differentiation to evaluate the pluripotent differentiation potential of NSCs.

Soft Agar Colony Formation Assay: NSCs single cell suspensions were mixed with 1.2% soft agar in NSCs culture medium. 3 × 103 NSCs were seeded into 6-well plate, each well supplemented with 2 mL NSCs culture medium. Every three days replaced supplemented medium. After 10 days, the colonies were photographed.

Isolation and Identification of NSCs-EVs: The supernatant was collected every three days during NSCs culture, and the dead cells and cell fragments were removed by centrifugation (300 g 10 min, 2000 g 30 min, and 10 000 g 30 min). Then, the supernatant was filtered by 0.22 µm membrane and ultracentrifuged at 100 000 g (Beckman L-90K, Pasadena, CA) for 70 min at 4 °C. Finally, the pellet was collected, washed with cold PBS at 100 000 g for 70 min, and then suspended for further testing. The equal volumes of medium without cells were ultracentrifuged to collect the pellet, and the protein concentration in fresh medium was 20% of the concentration in cell culture medium. BCA protein assay kit (Beyotime Biotechnology, Shanghai, China) was used to analyze the protein concentration of EVs. Then, the EVs were identified by transmission electron microscopy (Tecnai G2 SpiritBiotwin, Fisher Scientific, Waltham, MA), nanoparticle tracking analysis (ZetaView Particle Metrix, Inning am Ammersee, GER), and western blotting. Cell mitochondrial isolation kit (Beyotime Biotechnology, Shanghai, China) was used to isolate mitochondria from NSCs. To label EVs, PKH26 dye was used according to the instruction manual (Sigma–Aldrich, Waltham, MA). The PKH26-labeled EVs were washed at 100 000 g for 70 min, and collected. Then the EVs were diluted in Gel (1 µg $µL^{-1}$) and used for release experiment and cell uptake experiment.

Release Curve of EVs in Gel: Gel (100 µL) loaded with NSCs-EVs (1 µg $µL^{-1}$) was incubated with 1 mL glucose solution (100 mg dL^{-1}, 200 mg dL^{-1}, and 300 mg dL^{-1}) or hydrogen peroxide solution (100 and 200×10^{-6} M) for 12 days. The solution was changed every 24 h, and then the number of EVs that released from Gel-EVs were detected by NTA assay. After 12 days, the hydrogel was completely degraded, and the number of EVs particles released at each time point was calculated.

Scratch Wound Healing Assay: About 6×10^5 HUVECs were seeded in 6-well plate in triplicate and allowed to reach confluence. Confluent monolayer cells were treated with 10 µg mL^{-1} mitomycin to inhibit cell proliferation (Hisun Pharmaceutical Co. LTD, Tai Zhou, China) for 3 h. Then, a scratch was made in each well by a sterile pipette tip. Each group was cultured with 2 mL medium containing degradation products of hydrogel (60 µL), of Gel-EVs (60 µL, 1 µg $µL^{-1}$), as well as CM-V (60 µL, 0.2 µg $µL^{-1}$) and EV (60 µL, 1 µg $µL^{-1}$) to determine the migration rate of HUVECs, the distance of the wounded area at the selected position was measured at intervals of 24 h.

Tube Formation Analysis: Cold Matrigel (80 µL) (BD Biosciences, USA) was added into 48-well plate, and spread evenly on the bottom. Then 2×10^4 HUVECs were added into each well, and incubated at 37 °C incubation to solidify the gel. The potential of tube formation of HUVECs in different groups was observed by a microscope after 6 h of culture with 200 µL medium containing degradation products of hydrogel (6 µL), of Gel-EVs (6 µL, 1 µg μL^{-1}), as well as CM-V (6 µL, 0.2 µg μL^{-1}) and EV (6 µL, 1 µg μL^{-1}), respectively.

Brain Ischemic Stroke Mouse Model and EVs Treatment: Type 2 diabetes mellitus mice were induced by feeding high-fat diet and continuous intraperitoneal injection of sterile citrate buffer containing streptozotocin (25 mg kg^{-1} body weight, Sigma–Aldrich) for 5 days. Mice with glucose levels ≥300 mg dL^{-1} were classified as diabetes and used for producing a distal middle cerebral artery occlusion ischemia model according to the previously described method.[44] Briefly, diabetic mice were anesthetized with 2–3% isoflurane, the temporalis muscle was bisected through an incision midway between the eye and the ear. The proximal MCA was exposed through a subtemporal craniectomy and occluded by electrocautery hemostat. To monitor the in vivo biodistribution of EVs, 5×10^{-6} M DiR (Meilum Biotechnology, China) was used to label the EVs. Mice were randomly divided into seven groups: Healthy group, PBS group (10 µL PBS), Gel group (10 µL Gel), CM-V group (2 µg vesicles in 10 µL PBS), CG-EV group (10 µg EVs in 10 µL CG), EVs group (10 µg EVs in 10 µL PBS), and Gel-EV group (10 µg EVs in 10 µL Gel). Each group was then transplanted into the cortex of the infarcted hemisphere by using the coordinates: anterior–posterior (*A–P*), −0.5 mm; medial–lateral (*M–L*), 3 mm; and dorsal–ventral (*D–V*), 2 mm at 24 h after stroke onset. The injections were delivered at 1 µL min^{-1} and the needle was maintained in situ for 5 min post-injection, followed by slow removal.

Behavior Tests and Infarct Volume Analysis: Sticky tape test and grid walking test were used to assess the motor function and coordination of mice after stroke. Before surgery, the animals were subjected to a 3 days of tape removal training. Mice were briefly restrained and a rectangular piece of tape was placed on the bottom of each forepaw. Mice were then released, and the latency to remove the right forepaw tape was recorded. In grid walking test, mice were placed in the center of apparatus consisting of an elevated 20 × 40 cm metal grid with grid cells measuring 1.2 × 1.2 cm and were free to explore for 3 min. The total number of right footsteps and the total number of right foot-fault errors were recorded. The fault rate of the test was calculated by dividing the number of errors by the number of total steps and presented as the % foot fault rate. The neurobehavioral analysis was performed by sticky tape test and grid walking test at 1, 3, 7, and 14 days after stroke. 14 days after stroke, the mice were anesthetized, the thorax was exposed and the heart was perfused sequentially from left ventricle with PBS and 4% paraformaldehyde (Sinopharm Chemical Reagent, Shanghai, China). Mice brains were dissected out, fixed with 4% paraformaldehyde and dehydrated with 30% sucrose solution. A series of 30 µm thick brain sections with a total thickness of nearly 3.6 mm were collected, and the brain sections were stained with cresyl violet solution (Meilum Biotechnology, Da Lian, China). The stained sections were observed with a microscope and the volume of the ipsilateral and the ischemic hemispheres were calculated by ImageJ. The ischemic brain volume was estimated by the following formula: $V = \sum h/3\ [\Delta S_n + (\Delta S_n * \Delta S_{n+1})\ 1/2 + \Delta S_{n+1}]$. In the formula, V represents the volume, h represents the distance between two adjacent brain slices, and ΔS_n and ΔS_{n+1} represent different areas between two adjacent slices.

Immunofluorescence Staining and Immunohistochemistry: For immunofluorescence staining, NSCs and brain sections were fixed with 4% paraformaldehyde for 15 min at room temperature, and blocked with 1% bovine serum albumin (Sigma). Then the sections were incubated with primary antibodies against Nestin (Millipore, Burlington, MA), Tuj1 (Millipore, Burlington, MA), GFAP (Millipore, Burlington, MA), CD31 (R&D, Minneapolis, MN), and Ki67 (Abcam, Cambridge, UK) at 4 °C overnight. After that, the sections were washed three times with PBS and incubated with secondary antibody (Invitrogen, Carlsbad, CA). At last, brain sections were counterstained with DAPI (Life Technologies, Carlsbad, CA) and imaged using confocal fluorescence microscope (Leica, Solms, Germany). The immunohistochemistry results were analyzed by counting the number of CD31-positive vessels in the damaged cortex of each brain sections, with three brain sections (90 µm apart) in each mouse, four mice per group.

miRNA Sequencing and Analysis: The miRNA sequencing of NSCs-EVs was conducted by OE biotech Co., Ltd. (Shanghai, China). The known miRNAs were identified by aligning against miRbase v.21 database. The differentially expressed miRNAs were identified with the threshold of *p*-value <0.05, and then calculated with DEG algorithm. NSCs miRNAs were ranked according to average read counts of three samples (highest to lowest). The VEGF signaling pathway (KEGG 0 4370) related miRNAs were predicted by DIANA Tools and analyzed in three methods (Tarbase, microT, and Targetscan), and the intersection of predicted miRNAs datasets via three methods were obtained by Venn. The heat-map of miRNAs expression of NSCs-EVs and Fibroblast-EVs was drawn using OE biotech cloud platform. The scale represents signal intensity of log2 (TPM) values.

Statistical Analysis: All the statistical analysis was performed using GraphPad Prism 9.0 (GraphPad Software, La Jolla, CA) software. Results between experimental groups were analyzed by using post-hoc test with one-way analysis of variance (ANOVA). All error bars represent the mean±s.d. $^*p < 0.05$, $^{**}p < 0.01$, and $^{***}p < 0.001$. Sample size (n) for each statistical analysis was included in the figure legend.

Supporting Information

Supporting Information is available from the Wiley Online Library or from the author.

Acknowledgements

Y. J. and R. W. contributed equally to this work. This study was supported by grants from National Key R&D Program of China #2019YFA0112000 (YT), the National Natural Science Foundation of China (NSFC) projects 82071284 (YT), 81771251 (GYY), 81771244 (ZZ), 81974179 (ZZ), the Scientific Research and Innovation Program of Shanghai Education Commission 2019-01-07-00-02-E00064 (GYY), Science and Technological Innovation Act Program of Shanghai Science and Technology Commission, 20JC1411900 (GYY), the Natural Science Foundation of Shanghai 19ZR1437800 (HX).

Conflict of Interest

The authors declare no conflict of interest.

Data Availability Statement

The data that support the findings of this study are available from the corresponding author upon reasonable request.

Keywords

angiogenesis, brain microenvironment responsive hydrogels, diabetes, neural stem cell-derived extracellular vesicles, stroke

Received: May 15, 2022
Revised: August 26, 2022
Published online:

[1] M. Katan, A. Luft, *Semin Neurol* **2018**, *38*, 208.
[2] M. J. Luitse, G. J. Biessels, G. E. Rutten, L. J. Kappelle, *Lancet Neurol.* **2012**, *11*, 261.
[3] J. Chen, X. Cui, A. Zacharek, Y. Cui, C. Roberts, M. Chopp, *Stroke* **2011**, *42*, 445.

[4] M. M. Elgebaly, J. Arreguin, N. Storke, *J Stroke Cerebrovasc Dis* **2019**, *28*, 1413.
[5] E. Osei, S. Fonville, A. A. Zandbergen, P. J. Koudstaal, D. W. Dippel, H. M. den Hertog, *Acta Neurol. Scand.* **2017**, *135*, 170.
[6] C. Savopoulos, G. Kaiafa, I. Kanellos, A. Fountouki, D. Theofanidis, A. I. Hatzitolios, *J Endocrinol Invest* **2017**, *40*, 457.
[7] X. Fan, J. Qiu, Z. Yu, H. Dai, A. B. Singhal, E. H. Lo, X. Wang, *Stroke* **2012**, *43*, 567.
[8] J. D. Bernstock, L. Peruzzotti-Jametti, D. Ye, F. A. Gessler, D. Maric, N. Vicario, Y. J. Lee, S. Pluchino, J. M. Hallenbeck, *J Cereb Blood Flow Metab* **2017**, *37*, 2314.
[9] G. L. Zhang, Z. H. Zhu, Y. Z. Wang, *World J Stem Cells* **2019**, *11*, 817.
[10] G. Zhang, Z. Zhu, H. Wang, Y. Yu, W. Chen, A. Waqas, Y. Wang, L. Chen, *J Adv Res* **2020**, *24*, 435.
[11] T. R. Doeppner, J. Herz, A. Görgens, J. Schlechter, A. K. Ludwig, S. Radtke, K. de Miroschedji, P. A. Horn, B. Giebel, D. M. Hermann, *Stem Cells Transl Med* **2015**, *4*, 1131.
[12] O. Y. Bang, E. H. Kim, *Front Neurol* **2019**, *10*, 211.
[13] a) F. Zhao, D. Wu, D. Yao, R. Guo, W. Wang, A. Dong, D. Kong, J. Zhang, *Acta Biomater.* **2017**, *64*, 334; b) Z. Xu, G. Liu, J. Huang, J. Wu, *ACS Appl. Mater. Interfaces* **2022**, *14*, 7680.
[14] a) P. A. Hyslop, Z. Zhang, D. V. Pearson, L. A. Phebus, *Brain Res.* **1995**, *671*, 181; b) J. P. Wei, Q. H. Wang, H. J. Zheng, F. Wei, *Chin. J. Integr. Med.* **2018**, *24*, 723.
[15] N. Urbán, F. Guillemot, *Front Cell Neurosci* **2014**, *8*, 396.
[16] N. Urbán, I. M. Blomfield, F. Guillemot, *Neuron* **2019**, *104*, 834.
[17] G. Saravanakumar, J. Kim, W. J. Kim, *Adv. Sci.* **2017**, *4*, 1600124.
[18] M. Hatakeyama, I. Ninomiya, M. Kanazawa, *Neural Regen Res* **2020**, *15*, 16.
[19] P. Carmeliet, R. K. Jain, *Nature* **2011**, *473*, 298.
[20] A. Kuehbacher, C. Urbich, A. M. Zeiher, S. Dimmeler, *Circ. Res.* **2007**, *101*, 59.
[21] a) R. L. Webb, E. E. Kaiser, S. L. Scoville, T. A. Thompson, S. Fatima, C. Pandya, K. Sriram, R. L. Swetenburg, K. Vaibhav, A. S. Arbab, B. Baban, K. M. Dhandapani, D. C. Hess, M. N. Hoda, S. L. Stice, *Transl Stroke Res* **2018**, *9*, 530; b) R. L. Webb, E. E. Kaiser, B. J. Jurgielewicz, S. Spellicy, S. L. Scoville, T. A. Thompson, R. L. Swetenburg, D. C. Hess, F. D. West, S. L. Stice, *Stroke* **2018**, *49*, 1248.
[22] J. Lam, N. F. Truong, T. Segura, *Acta Biomater.* **2014**, *10*, 1571.
[23] Z. Wu, B. Kong, R. Liu, W. Sun, S. Mi, *Nanomaterials* **2018**, *8*.
[24] J. M. Barnes, L. Przybyla, V. M. Weaver, *J. Cell Sci.* **2017**, *130*, 71.
[25] W. Shi, B. Hass, M. A. Kuss, H. Zhang, S. Ryu, D. Zhang, T. Li, Y. L. Li, B. Duan, *Carbohydr. Polym.* **2020**, *233*, 115803.
[26] A. C. Gaffey, M. H. Chen, A. Trubelja, C. M. Venkataraman, C. W. Chen, J. J. Chung, S. Schultz, C. M. Sehgal, J. A. Burdick, P. Atluri, *J Thorac Cardiovasc Surg* **2019**, *157*, 1479.
[27] a) M. M. Bastings, S. Koudstaal, R. E. Kieltyka, Y. Nakano, A. C. Pape, D. A. Feyen, F. J. van Slochteren, P. A. Doevendans, J. P. Sluijter, E. W. Meijer, S. A. Chamuleau, P. Y. Dankers, *Adv. Healthcare Mater.* **2014**, *3*, 70; b) E. Alarçin, T. Y. Lee, S. Karuthedom, M. Mohammadi, M. A. Brennan, D. H. Lee, A. Marrella, J. Zhang, D. Syla, Y. S. Zhang, A. Khademhosseini, H. L. Jang, *Biomater. Sci.* **2018**, *6*, 1604.
[28] J. H. Lee, *Biomater. Res.* **2018**, *22*, 27.
[29] K. L. Wilson, S. T. Carmichael, T. Segura, *J Vis Exp* **2020**, *164*, e61450.
[30] A. Akbari, N. Jabbari, R. Sharifi, M. Ahmadi, A. Vahhabi, S. J. Seyedzadeh, M. Nawaz, S. Szafert, M. Mahmoodi, E. Jabbari, R. Asghari, J. Rezaie, *Life Sci.* **2020**, *249*, 117447.
[31] a) K. Zhang, X. Zhao, X. Chen, Y. Wei, W. Du, Y. Wang, L. Liu, W. Zhao, Z. Han, D. Kong, Q. Zhao, Z. Guo, Z. Han, N. Liu, F. Ma, Z. Li, *ACS Appl. Mater. Interfaces* **2018**, *10*, 30081; b) C. Han, J. Zhou, C. Liang, B. Liu, X. Pan, Y. Zhang, Y. Wang, B. Yan, W. Xie, F. Liu, X. Y. Yu, Y. Li, *Biomater. Sci.* **2019**, *7*, 2920.
[32] I. S. Arts, A. Gennaris, J. F. Collet, *FEBS Lett.* **2015**, *589*, 1559.
[33] Y. Zhang, Y. Zhang, M. Chopp, Z. G. Zhang, A. Mahmood, Y. Xiong, *Neurorehabil Neural Repair* **2020**, *34*, 616.
[34] R. Prakash, W. Li, Z. Qu, M. A. Johnson, S. C. Fagan, A. Ergul, *Stroke* **2013**, *44*, 2875.
[35] A. Ergul, J. P. Valenzuela, A. Y. Fouda, S. C. Fagan, *Brain Res.* **2015**, *1623*, 81.
[36] G. E. Manuel, T. Johnson, D. Liu, *Int J Physiol Pathophysiol Pharmacol* **2017**, *9*, 188.
[37] A. Tiwari, B. Mukherjee, M. Dixit, *Curr. Cancer Drug Targets* **2018**, *18*, 266.
[38] Y. Zhu, J. Zhang, X. Hu, Z. Wang, S. Wu, Y. Yi, *Sci. Rep.* **2020**, *10*, 5313.
[39] W. Dhahri, S. Dussault, P. Haddad, J. Turgeon, S. Tremblay, K. Rolland, M. Desjarlais, K. Y. Cáceres-Gorriti, R. Mathieu, A. Rivard, *J. Cell. Mol. Med.* **2017**, *21*, 2211.
[40] J. Chen, R. Ning, A. Zacharek, C. Cui, X. Cui, T. Yan, P. Venkat, Y. Zhang, M. Chopp, *Stem Cells* **2016**, *34*, 102.
[41] D. Y. Lee, Z. Deng, C. H. Wang, B. B. Yang, *Proc Natl Acad Sci U S A* **2007**, *104*, 20350.
[42] D. Zhong, Y. Cao, C. J. Li, M. Li, Z. J. Rong, L. Jiang, Z. Guo, H. B. Lu, J. Z. Hu, *Exp. Biol. Med.* **2020**, *245*, 54.
[43] F. H. Moghadam, M. Sadeghi-Zadeh, B. Alizadeh-Shoorjestan, R. Dehghani-Varnamkhasti, S. Narimani, L. Darabi, A. K. Esfahani, M. H. Nasr Esfahani, *J Vis Exp* **2018**, *141*, e58874.
[44] K. P. Doyle, M. S. Buckwalter, *Methods Mol Biol* **2014**, *1135*, 103.